JOURNAL OF APPLIED ELECTROCHEMISTRY 9 (1979) 101–108

Electrolysis in an annular flow cell with gas generation

T. Z. FAHIDY

Department of Chemical Engineering, University of Waterloo, Waterloo, Ontario, Canada

Received 7 April 1978

A cylindrical electrochemical cell with axial flow in the annulus, formed by the inner indifferent anode tube and the outer cathode tube, is analysed in terms of various reactor models. One alternative characterization, the radial dispersion model, allows the estimation of an apparent radial dispersion on the basis of experimental conversion data.

Nomenclature

- a ratio of the inner electrode radius to the outer electrode radius
- c active ion concentration; c_0 same in bulk
- d_e equivalent (or hydraulic) diameter
- D_i ionic diffusion coefficient
- D_r radial dispersion coefficient
- F Faraday's constant
- i_z current density distribution along the cathode
- J_n Bessel function of the first kind, order n
- I current flow between the electrodes; I_m its mean value
- L length of the cathode
- n number of electrons transferred in the cathode reaction
- p eigenvalue set in the Annular Hankel Transform
- Q volumetric flow rate of electrolyte
- r radius
- R_i radius of the inner electrode (anode)
- R_o radius of the outer electrode (cathode)
- (Re) Reynolds number (characteristic length: hydraulic diameter)
- S dimensionless radius, r/R_o
- S_i stoichiometric number
- (Sc) Schmidt number
- u_m mean value of electrolyte linear velocity
- x conversion, defined as $(c_0 - c)/c_0$; x_E average exit conversion; $\hat{x}_E$: x_E computed from a regression line; x_w conversion at the cathode tube
- y dimensionless axial variable, z/L
- Y_n Bessel function of the second kind, order n
- z axial coordinate
- α degree of dissociation
- β lumped parameter in radial dispersion model
- ϕ geometric-aspect parameter in annulus flow theory
- τ electrolyte residence time in cell

1. Introduction

Annular flow has been used as a convenient means of studying mass transport occurring in concentric-cylinder reactors with dominating axial fluid motion; the state of art has recently been reviewed by Newman [1] and Pickett [2]. While relatively numerous experimental studies have been carried out with this geometry, current understanding of the annular-flow reactor is still rather limited, especially in the case of long electrodes and where axial and radial dispersion can play a significant, if not predominant, role. Fully laminar and fully turbulent hydrodynamic regimes have been postulated for pertinent mathematical models with simplified electrode processes; the instance of fast electrochemical kinetics has received more detailed attention [3].

In this paper the behaviour of an annular-flow concentric-cylinder electrochemical reactor is analyzed; this reactor has sufficiently different characteristics from those previously described in the literature, in the following sense: the inner and outer annulus walls are fully active electrodes; the reactor length/hydraulic diameter ratio is large; the electrolyte concentration is very low; and finally, there is gas evolution at the electrodes as a result of

the parallel electrochemical reactions occurring at both anode and cathode. As shown in the sequel, no simple hydrodynamic model applies without reservations, and, indeed, the analysis lends itself to various interpretations of the mass transport phenomena inherent to such a cell.

2. Experimental

A sketch of the experimental apparatus is shown in Fig. 1. The cell consists of a 55 cm long copper cathode tube of inside diameter 12·8 mm and a 60 cm long, 5 mm-diameter lead anode rod placed in the axis of the cathode tube; the hydraulic diameter of the annulus is 7·8 mm. The relatively small cell size was chosen in order to effect relatively small volumetric throughput rates within the range of the linear velocities employed. The cell was supported at the bottom and on the top by two plexiglass blocks which also served for holding the electrical connections. The electrolyte was circulated by means of a centrifugal pump between the mixing tank, the head tank and the cell; the electrolyte flow rate was measured and monitored via a calibrated rotameter. Electrolysis was carried out by using standard laboratory-scale regulated power supplies whose generated current flow was measured with a calibrated shunt-resistor. The range of the inlet electrolyte composition was 0·26–0·3 mM l^{-1} Cu^{2+} (about 16·6–19·1 ppm) in deionized water; the range of dilution was chosen to ensure measureable changes in the Cu(II) ion concentration in the electrolyte over relatively small time periods and to ensure H_2 generation parallel to the reduction of Cu(II) ions at the cathode at relatively low current flows. The electrolyte temperature was kept between 293 –297 K; the flow rate was varied between 25–200 $cm^3 min^{-1}$. The inflow and effluent copper ion content was determined by conventional absorption spectroscopy, using analytical-grade Cu^{2+} standards and an associated concentration–absorbance curve. The experiments were performed at constant flow rates and at galvanostatic conditions, with the effluent concentration analysed at five- and ten-minute intervals after starting. The cell and electrode surfaces were meticulously cleaned after each experiment.

Fig. 2 shows typical variations of the experimentally obtained exit conversion with the electrolyte residence time at two distinct current densities. Each set of data is a combination of the five-minute and ten-minute lapse results inasmuch as pertinent likelihood-ratio analysis [4] (or, alternatively, the Neyman-Pearson [5, 6] L_1-parameter test) indicates that at a 95% confidence level the lapse-time effect is statistically indistinguishable and thus, the cell has reached steady-

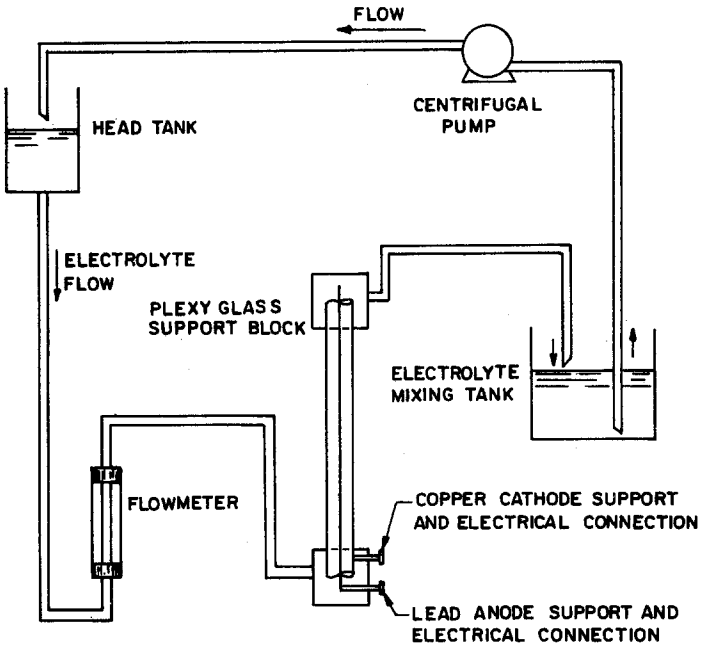

Fig. 1. Layout of the experimental apparatus.

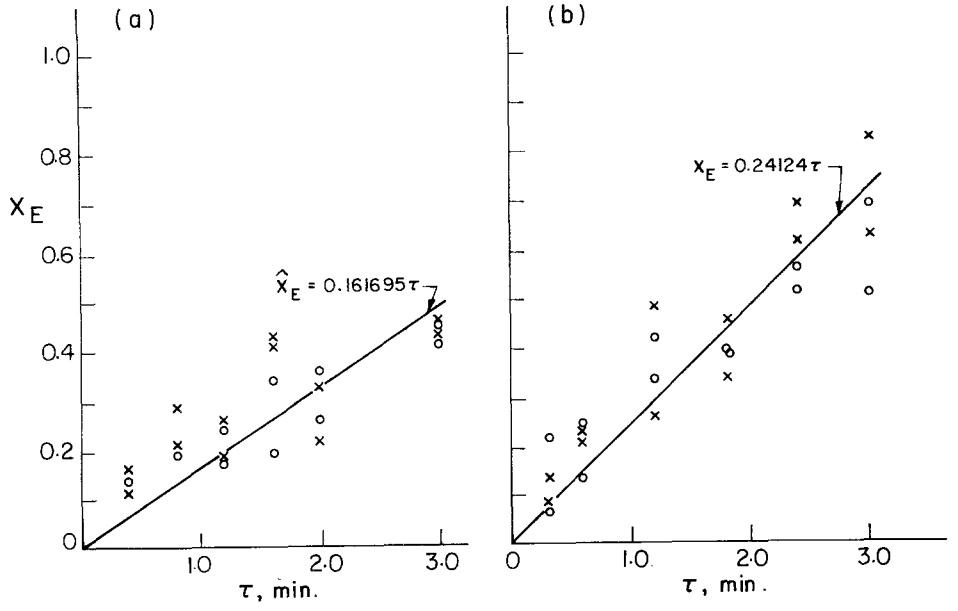

Fig. 2. Experimental exit conversion versus electrolyte residence time data at (a) 50 mA and (b) 300 mA current flow. The solid lines are regression relationships. The symbols correspond to chemical analysis performed at 5 min (X) and 10 min(•) from the start of electrolysis.

state conditions. The scatter of the conversion values is partially due to relatively close inflow and effluent concentrations which make the computed conversion especially sensitive to measurement errors related to absorption spectroscopy.

Another source of scatter is the local blanketing effect of the generated oxygen gas on the anode and of the hydrogen gas at the cathode whose magnitude and distribution varies with electrolyte flow rate and the electric current flow. The least-squares regression lines and associated 90%-level confidence intervals for the slope were computed as

$$\hat{x}_E = 0{\cdot}1617\tau;\ [0{\cdot}1455 - 0{\cdot}1779] \text{ at } I = 50\,\text{mA} \quad (1)$$

$$\hat{x}_E = 0{\cdot}2412\tau;\ [0{\cdot}2231 - 0{\cdot}2594] \text{ at } I = 300\,\text{mA} \quad (2)$$

with associated standard errors of estimate of 0·07723 and 0·09379, respectively. These results indicate that the exit conversion varies essentially in a linear fashion with the electrolyte residence time regardless of the current flow maintained in the cell, although the magnitude of variation is, as expected, related to the current density.

3. General analysis of the experimental results

3.1. *The electrode reactions*

In the $I = 50$ mA runs, the cell voltage drop varied between 5·3–6 V and in the $I = 300$ mA runs between 15–24 V. Since the calculated value of the motionless, gas-free electrolyte resistance between the two electrodes is 40·9 Ω, both electrodes were strongly polarized in their respective (i.e., anodic and cathodic) directions, in spite of additional voltage drops taken up by the generated gas layers. Under such conditions, several anode and cathode reactions may take place, and their thermodynamic probability may be ascertained via the well-known Pourbaix diagrams [17] of Cu and Pb. On the anode, the major reaction is oxygen evolution:

$$2H_2O = O_2 + 4H^+ + 4e^- \quad (3)$$

whose potential is estimated to be 0·814 V under experimental conditions (pH ~ 7). The overvoltage of oxygen on precipitated Pb powder may be computed [18] as 0·68 V at $I = 50$ mA ($2{\cdot}26\ \text{A m}^{-2}$) and 0·85 V at $I = 300$ mA ($13{\cdot}56\ \text{A m}^{-2}$); on a solid lead anode similar over-

voltage values may be expected. Consequently, at such potentials and under the given experimental conditions the reactions

$$Pb = Pb^{2+} + 2e^- \quad E = -0{\cdot}233\,V \tag{4}$$

$$Pb + H_2O = PbO + 2H^+ + 2e^-$$

$$E = -0{\cdot}155\,V \tag{5}$$

$$3PbO + H_2O = Pb_3O_4 + 2H^+ + 2e^-$$

$$E = 0{\cdot}525\,V \tag{6}$$

$$Pb^{2+} + 2H_2O = PbO_2 + 4H^+ + 2e^-$$

$$E = 0{\cdot}743\,V \tag{7}$$

appear thermodynamically feasible (the Pb^{2+} ion concentration was estimated from the $PbSO_4$ solubility product, 2×10^{-8}, as $7{\cdot}646 \times 10^{-5}$ $mol\,l^{-1}$ at equilibrium conditions). Since the electrolyte contains a very small amount of sulphate ion, the $Pb + SO_4^{2-} = PbSO_4 + 2e^-$ reaction is rather improbable, so is its concomitant, the $PbSO_4 \rightarrow Pb^{2+} + SO_4^{2-}$ process.

On the cathode, several electrode processes involving copper, and hydrogen evolution can take place. For the formula average Cu(II) ion concentration of about $2{\cdot}8 \times 10^{-4}\,mol\,l^{-1}$, using ion-association data [19; pK = 2·37, $\alpha = 0{\cdot}835$], the electrolyte mean activity coefficient is estimated as $\gamma_{\pm} = 0{\cdot}9342$, hence the copper(II) ion activity as $2{\cdot}616 \times 10^{-4}\,mol\,l^{-1}$. Hence, the reduction process

$$Cu^{2+} + 2e^- = Cu \tag{8}$$

has an estimated potential of 0·232 V. Under the experimental conditions, the reactions

$$Cu^{2+} + e^- = Cu^+ \quad E = 0{\cdot}153\,V \tag{9}$$

$$2Cu^+ + H_2O = Cu_2O + H^+ + 2e^-$$

$$E = 0{\cdot}0573\,V \tag{10}$$

$$Cu_2O + H_2O = 2CuO + 2H^+ + 2e^-$$

$$E = 0{\cdot}333\,V \tag{11}$$

are also feasible; the cathodic reduction of Pb(II) ions generated by the anode reactions discussed above is also possible in principle ($E_0 = -0{\cdot}247$ V). Hydrogen evolution is estimated to have the thermodynamic potential of −0·414 V in a pure H_2 atmosphere; under the experimental conditions the H^+ reduction potential is most likely about −0·34 to −0·37 V.

While thermodynamic considerations lead to a rather complicated picture, certain experimental observations allow appreciable simplifications. First, the ratio of Equations 2 and 1 being 1·49, a significant proportion of the cathode current in the 300 mA runs was spent for hydrogen generation. In these experiments an uneven glutinous layer of greenish appearance was found on the cathode surface at the termination of electrolysis, this layer often containing tiny black particles. Upon dissolution of the layer and particles, atomic absorption tests of the solution aliquot indicated no detectable presence of lead ions; in consequence, it is most likely that hydrogen generation and copper deposition are the only cathode processes of importance. From the relatively large rate of hydrogen evolution at the cathode one can safely assume that the copper(II) ion concentration at the cathode is essentially zero and the deposition process is essentially mass-transfer controlled; thus, copper deposition is the limiting process for which the reduction of H^+ ions serves as 'background' current; the major role of gas evolution at both electrodes is in establishing a characteristic hydrodynamic and convective regime in the cell.

With this background of the pertinent electrode processes in mind the behaviour of the cell will now be analysed in terms of electrochemical reaction engineering principles, by comparing the experimentally observed values of conversion with values predicted via selected hydrodynamic and mass transport models. Alternatively, model-predicted current flows may be compared to experimental current flows, wherever more convient.

3.2. *Backmix-flow model*

In terms of the average current flow, the conversion may be estimated [2, Equation 6.3] as

$$x_E = \frac{I_m}{nFQc_0}. \tag{12}$$

In the case of $I_m = 50$ mA, only in a small number of cases does Equation 12 yield $x_E < 1$; where $I_m = 300$ mA, all predicted values of x_E are larger

than unity. Since I_m includes the background current due to H^+ ion reduction, this finding is not surprising and it indicates that this model has little significance in interpreting the behaviour of this cell.

3.3. *Plug-flow model*

In concentric annulus flow the reacting-ion concentration gradient may be written [2, Equation 5.3] as

$$\frac{dc}{dz} = -\frac{2R_o i_z(z)}{u_m(R_o^2 - R_i^2)nF} \tag{13}$$

where $i_z(z)$ denotes the current density distribution along the cathode surface. If i_z is replaced by its surface-averaged value i_m, integration of Equation 13 leads to Equation 12; at the other extreme, if complete mass transport control is assumed at the cathode surface then the current distribution may be estimated as [1, Equation 105-1]

$$i_z = \frac{0{\cdot}8546\, nFc_0 D_i^{2/3}}{S_i}\left(\frac{\phi}{1-a}\right)^{1/3}\frac{u_m^{1/3}}{R_o^{1/3}z^{1/3}} \tag{14}$$

where ϕ is related to the outer electrode as cathode. Notice that Equation 14 may be used since the condition $L/2R_o \ll (Re)(Sc)$ is satisfied ($L/R_o = 42{\cdot}97$, whereas $3{\cdot}72 \times 10^4 < (Re)(Sc) < 3{\cdot}56 \times 10^5$ in the experimental cell; see sequel); alternatively [1, Equation 105-4], $L < 0{\cdot}005\,(Re)(Sc)d_e$, the latter being between 1·45–13·9 m. Thus, Equation 13 can be integrated to the final form of

$$x_E = 2{\cdot}5638\,\frac{R_o^{2/3}L^{2/3}D_i^{2/3}}{(R_o^2 - R_i^2)u_m^{2/3}S_i}\left(\frac{\phi_0}{1-a}\right)^{1/3}. \tag{15}$$

At 25° C, the average diffusion coefficient for the electrolyte concentration range is estimated to be about $D_i \cong 6{\cdot}4 \times 10^{-6}\,cm^2\,s^{-1}$ and Equation 15 predicts a conversion range of $0{\cdot}0173 \leqslant x_E \leqslant 0{\cdot}0787$, which is much too conservative, in view of the experimental observations.

3.4. *Annulus flow models*

The conventional dimensionless mass transport equations proposed for short electrodes in fully developed laminar flow [1] predict very small current flows (0·38–0·8 mA) in the cell in spite of transference-number corrections. Using a heat transport model for the 'long-electrode' case in fully developed laminar flow [7, 8] the predicted current flow range is 0·8–3·9 mA. On the other hand, if turbulent-flow models are considered, such as the classical Chilton–Colburn equation [9, 1: Equation 105-13; 2: Equation 4.76] the apparent Reynolds number range is computed as $1{\cdot}03 \times 10^5$–$2{\cdot}47 \times 10^6$. It is then obvious from the foregoing that gas evolution results in strongly turbulent bulk conditions, and behaviour in the neighbourhood of the cathode may be interpreted via radial dispersion concepts.

3.5. *Analysis via dispersion effects*

For the sake of completeness axial dispersion effects will first be examined. If there were no gas evolution in the cell, the axial Peclet number could be crudely estimated [10] to be in the range of $0{\cdot}038 \leqslant (Pe)_L \leqslant 0{\cdot}364$; however, since $d_e^2/D_i \gg \tau_{ave}$, the time constant associated with radial diffusion is much larger than the average residence time and it follows that axial dispersion is of little importance in this system; gas evolution-generated local mixing strengthens this conclusion. It is more inviting, therefore, to assign a dispersion-induced concentration distribution to the direction transverse to axial flow and consider radial dispersion as a governing phenomenon. The corresponding mass balance may be written as

$$u_m\frac{\partial c}{\partial z} = D_r\left(\frac{\partial^2 c}{\partial r^2} + \frac{1}{r}\frac{\partial c}{\partial r}\right) \tag{16}$$

with appropriate boundary conditions related to R_o and R_i, and an initial (or boundary) condition related to $z = 0$ (or $z = L$).

4. An approximate radial dispersion model: estimation of the apparent radial dispersion coefficient

The mathematical complexity of solving Equation 16 is related to the initial and/or boundary conditions; easily manageable analytical solutions cannot be *a priori* guaranteed. The problem may be handled with relative ease, however, if it is assumed that the reacting-ion concentration is essentially constant along the electrode. Introducing dimensionless variables $z/L \equiv y$ and $r/R_o \equiv S$, Equation 16 may be rewritten as

$$\frac{1}{\beta}\frac{\partial x}{\partial y} = \frac{\partial^2 x}{\partial S^2} + \frac{1}{S}\frac{\partial x}{\partial S}; \quad \beta \equiv \frac{LD_r}{R_o^2 u_m} \tag{17}$$

with auxiliary conditions

$$y = 0; \quad x = 0 \tag{18}$$

$$S = a; \quad x = 0; \quad a = R_i/R_o \tag{19}$$

$$S = 1; \quad x = x_w \tag{20}$$

As shown in the Appendix, the solution may be obtained via the Annular Hankel Transform (AHT) technique as [11, 12]

$$\frac{x(y,S)}{x_w} = \pi \sum_p \frac{1-\epsilon^{-\beta p^2 y}}{J_0^2(pa) - J_0^2(p)} J_0(pa) J_0(p) B_0(pS) \tag{21}$$

hence

$$\frac{x_E}{x_w} = \frac{2\pi}{1-a^2} \sum_p (1-\epsilon^{-\beta p^2}) N(p) Q(p) \tag{22}$$

where

$$N(p) \equiv \frac{J_0(pa)J_0(p)}{J_0^2(pa) - J_0^2(p)} \tag{23}$$

$$Q(p) \equiv \int_a^1 S B_0(pS)\, dS \tag{24}$$

$$B_0(pS) \equiv J_0(pS)Y_0(pa) - Y_0(pS)J_0(pa) \tag{25}$$

and p are the positive ascending roots of the equation

$$J_0(p)Y_0(pa) = Y_0(p)J_0(pa) \tag{26}$$

Fig. 3 is a 'template' plot of $\chi = [(1-a^2)/2\pi] \times (x_E/x_w)$ against β for the experimental radius ratio $a = 0{\cdot}391$; this parameter determines the numerical value of the eigenvalue set.

On account of the analysis in Section 3.1, x_w may be taken to be 1·0 as a reasonable approximation; then using the experimentally observed exit conversion values and Fig. 3, β is about $4{\cdot}15 \times 10^{-3}$ at $I = 50$ mA and $u_m = 2{\cdot}934$ cm s^{-1}, and it approaches infinity at $I = 300$ mA and low u_m values (about 0·31 cm s^{-1}). Thus, the lower-end limiting value of the apparent radial dispersion coefficient is about $D_r = 7 \times 10^{-5}$ cm^2 s^{-1}, and the upper-end asymptotic value of infinity indicates that near backmix-flow conditions prevail in the cell, at low electrolyte flow rates and relatively large current flows. It is instructive to consider the alternative form of Equation 21

$$\frac{x}{x_w} = \frac{1}{S}\left(\frac{S^2-a^2}{1-a^2}\right) - \pi \sum_p N(p) B_0(pS) \epsilon^{-\beta p^2 y}. \tag{27}$$

For an infinitely long reactor ($y \to \infty$) or infinitely fast radial dispersion and/or infinitely low electrolyte flow rates ($\beta \to \infty$) Equation 27 yields

$$\frac{x_E}{x_w} \to \frac{2}{3}\frac{1-3a^2+2a^3}{(1-a^2)^2}. \tag{28}$$

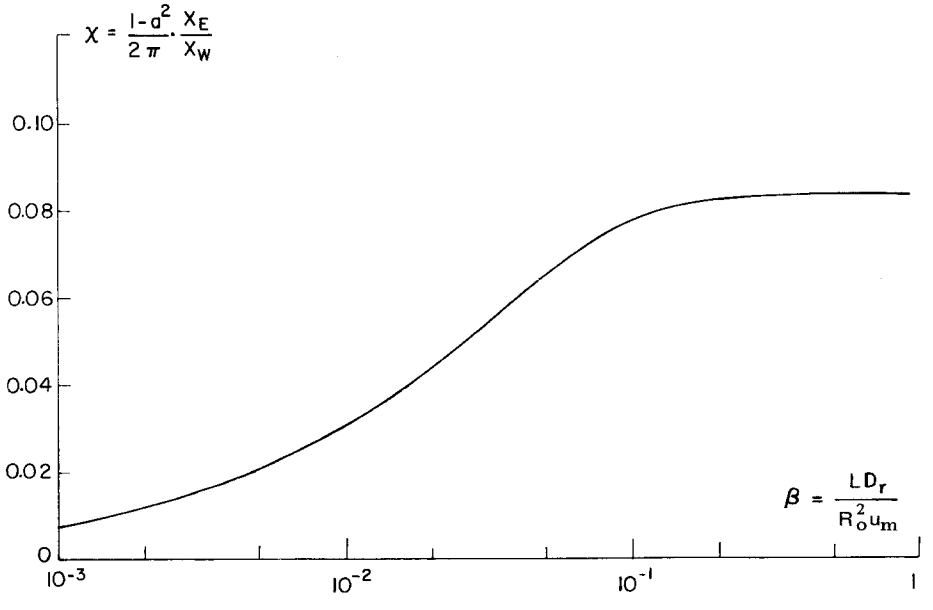

Fig. 3. χ-β plot for the estimation of the apparent radial dispersion coefficient for $R_i/R_o = 0{\cdot}391$.

For the experimental cell, $x_E/x_w \to 0{\cdot}614$ which agrees quite well with the value of 0·620 computed via Fig. 3; the slight discrepancy is due to truncation of the expansion in Equations 22–26 past the tenth root of Equation 26.

5. Further remarks

An interesting alternative to the radial dispersion approach is obtained if, in lieu of the condition in Equation 20, a finite concentration gradient, proportional to the reacting-ion concentration at the electrode is postulated. This condition, known as the 'radiation boundary condition' in the theory of partial differential equations, is also manifest in Damköhler's classical kinetic model of tubular reactors [13, 14] with plug-flow combined with radial diffusion. Only a small subset of the experimental cell data yields finite equivalent first-order reaction rate constants in the order of magnitude of $0{\cdot}3\ h^{-1}$; the rest of the conversion data would indicate essentially instantaneous kinetics. Hence the experimental cell performs better than an equivalent plug-flow reactor with radial diffusion, and first-order kinetics at the catalytic surface.

Finally, the analysis in Section 4 is considerably simplified for full-cylinder flow, which is the limiting case of $a \to 0$. Under such conditions, Equation 17 may be solved via Hankel transformation [11, Section 6.7] to the final expression

$$x_E = 1 - 4 \sum_n \frac{\epsilon^{-\beta\alpha_n^2}}{\alpha_n^2} \qquad (29)$$

where $J_0(\alpha_n) = 0$, i.e., α_n are the ascending roots of the J_0 function. For annulus cells of small R_i/R_o ratio, Equation 29 yields a much faster estimate than the rigorous analysis of Section 4.

In conclusion, electrochemical reactions in axial-flow annulus cells may be interpreted in terms of several reactor engineering models; with gas evolution at the electrodes, the radial dispersion model is one attractive means of analysis.

Appendix

The solution of Equation 17 via Annual Hankel Transformation (AHT)

The Annular Hankel Transform [11, 12] is generally defined as

$$\bar{f}(p) \equiv \int_a^b f(r) r B_n(pr)\, dr \qquad (A1)$$

where p is the transform parameter and the kernel is related to Bessel functions J_n and Y_n by the relationship

$$B_n(pr) = J_n(pr)Y_n(pa) - Y_n(pr)J_n(pa). \qquad (A2)$$

Let the operator $F(\psi)$ be defined as

$$F(\psi) \equiv \frac{1}{r}\frac{\partial}{\partial r}\left(r\frac{\partial \psi}{\partial r}\right) - \frac{n^2\psi}{r} \qquad (A3)$$

where ψ is some potential function (i.e., temperature, concentration, voltage drop, etc.). Then, applying the AHT technique, the relationship

$$\int_a^b F(\psi) r B_n(pr)\, dr = \frac{2}{\pi}\left[\psi_{r=b}\frac{J_n(pa)}{J_n(pb)} - \psi_{r=a}\right] - p^2\bar{F}(p) \qquad (A4)$$

is obtained; here $\bar{F}(p)$ is the AHT of ψ. The transform parameter p represents the set of eigenvalues obtained from solving Equation A5

$$J_n(pb)Y_n(pa) = Y_n(pb)J_n(pa). \qquad (A5)$$

Consider now the particular instance of Equation 17, whose right-hand side is identified as $F(x)$, provided $n = 0$. Moreover, in terms of the fractional conversion x/x_w, the problem becomes isomorphic to the classical hydrodynamic problem of viscous fluid motion between two concentric cylinders and it can be treated as shown in [11, Section 6.10], except that $n = 0$ (instead of $n = 1$ in the fluid flow problem). The transform yields the ordinary differential equation

$$\frac{1}{\beta}\frac{d\bar{x}}{dy} = \frac{2}{\pi}x_w\frac{J_0(pa)}{J_0(p)} - p^2\bar{x} \qquad (A6)$$

where $\bar{x}$ is the AHT of the conversion. Equation A6 may be solved by any standard technique to the form of

$$\overline{x(p)} = \frac{2x_w}{\pi}\frac{J_0(pa)}{p^2J_1(p)}(1 - \epsilon^{-\beta p^2 y}). \qquad (A7)$$

The inverse of an AHT may be written in general [11] as

$$f(r) = \frac{\pi^2}{2}\sum_p \frac{p^2J_n^2(pb)}{J_n^2(pa) - J_n^2(pb)} B_n(pr)\bar{f}(p) \qquad (A8)$$

hence, in this particular instance, inversion of Equation A7 yields

$$\frac{x(y, S)}{x_w} = \pi \sum_p \frac{J_0(pa)J_0(p)B_0(pS)}{J_0^2(pa) - J_0^2(p)}(1 - \epsilon^{-\beta p^2 y}) \tag{A9}$$

At the cell exit, $y = 1$; furthermore, the value of the conversion averaged over the cross-sectional flow area being of main interest, the inverse is finally obtained for

$$x_E \equiv \frac{1}{(R_o^2 - R_i^2)\pi} \int_{R_i}^{R_o} x(r)(2r\pi)\, dr$$

$$= \frac{2}{1 - a^2} \int_b^1 Sx(S)\, dS$$

as

$$x_E = \frac{2\pi}{1 - a^2} \sum_p \frac{1 - \epsilon^{-\beta p^2}}{J_0^2(pa) - J_0^2(p)} J_0(pa)J_0(p) \times \int_a^1 SB_0(pS)\, dS \tag{A10}$$

which is Equations 22–26.

The numerical computation of the eigenvalue set p was performed by a convenient expansion technique [15] rather than by a root-finding technique and using Bessel function tables; with respect to the limited experimental accuracy, the first ten values of the full eigenvalue set were used in constructing Fig. 3.

The application of the AHT technique to cylindrical electrochemical cell analysis has previously been introduced [16] in a somewhat different context.

Acknowledgment

S. Attlesey and T. S. Rutherford, recipients of a University of Waterloo Faculty of Engineering Undergraduate Scholarship, obtained the experimental data. The project was supported by the National Research Council of Canada.

References

[1] J. S. Newman, 'Electrochemical Systems', Prentice Hall, New Jersey (1973) Section 105.
[2] D. J. Pickett, 'Electrochemical Reactor Design', Elsevier, Amsterdam (1977) Sections 4.6, 5.2.
[3] *Idem, ibid* Section 5.12.
[4] P. G. Hoel, 'Introduction to Mathematical Statistics', John Wiley and Chapman and Hall (1956) Section 10.1.4.1.
[5] J. Neyman and E. S. Pearson, *Bull. acad. polon. sci. lettr.* A (1931).
[6] H. S. Mickley, T. K. Sherwood and C. E. Reed, 'Applied Mathematics in Chemical Engineering, McGraw Hill, New York, Section 2.10.
[7] M. Jakob and K. A. Rees, *Trans. AIChE* 37 (1941) 619.
[8] R. E. Lundberg, W. C. Reynolds and W. M. Kays, NASA TND-1972, Washington, DC, 1963.
[9] T. H. Chilton and A. P. Colburn, *Ind. Eng. Chem.* 26 (1934) 1183.
[10] H. Kramer and K. R. Westersterp, 'Elements of Chemical Reactor Design and Operation', Academic Press (1963) Section III.9.
[11] C. J. Tranter, 'Integral Transforms In Mathematical Physics', Methuen, London (1962) Ch. VI.
[12] I. N. Sneddon, *Phil. Mag.* 37 (1946) 17.
[13] G. Damköhler, *Z. Elektrochem.* 42 (1936) 846.
[14] T. Baron, W. R. Manning and H.F. Johnstone, *Chem. Engrg. Progr.* 48, (3) 1952) 125.
[15] M. Abramovitz and I. A. Stegun, 'Handbook of Mathematical Functions', Dover, New York (1972) Section 9.5.
[16] S. Mohanta and T. Z. Fahidy, *J. Appl. Electrochem.* 6 (1976) 211.
[17] M. Pourbaix, 'Atlas d'Equilibres Electrochimiques' Gauthier-Villars Paris (1963).
[18] G. Milazzo, 'Electrochime I', Dunod, Paris, (1969) Chapter IV.
[19] C. W. Davies, 'Ion Association', Butterworths, London (1962).